

Universal Cell Embeddings: A Foundation Model for Cell Biology

Yanay Rosen^{1,*}, Yusuf Roohani^{2,*}, Ayush Agrawal¹, Leon Samotorčan¹,
Tabula Sapiens Consortium³, Stephen R. Quake^{4,5,6,†}, Jure Leskovec^{1,†}

¹ Department of Computer Science, Stanford University, Stanford, CA, USA

² Department of Biomedical Data Science, Stanford University, Stanford, CA, USA

³ Chan Zuckerberg BioHub, San Francisco, CA, USA

⁴ Department of Bioengineering, Stanford University, Stanford, CA, USA

⁵ Department of Applied Physics, Stanford University, Stanford, CA, USA

⁶ Chan Zuckerberg Initiative, Redwood City, CA, USA

[†]Corresponding author. Email: jure@cs.stanford.edu, quake@stanford.edu

*These authors contributed equally

Abstract

Developing a universal representation of cells which encompasses the tremendous molecular diversity of cell types within the human body and more generally, across species, would be transformative for cell biology. Recent work using single-cell transcriptomic approaches to create molecular definitions of cell types in the form of cell atlases has provided the necessary data for such an endeavor. Here, we present the Universal Cell Embedding (UCE) foundation model. UCE was trained on a corpus of cell atlas data from human and other species in a completely self-supervised way without any data annotations. UCE offers a unified biological latent space that can represent any cell, regardless of tissue or species. This universal cell embedding captures important biological variation despite the presence of experimental noise across diverse datasets. An important aspect of UCE's universality is that any new cell from any organism can be mapped to this embedding space with no additional data labeling,

25 **model training or fine-tuning. We applied UCE to create the Integrated Mega-scale Atlas,**
26 **embedding 36 million cells, with more than 1,000 uniquely named cell types, from hundreds**
27 **of experiments, dozens of tissues and eight species. We uncovered new insights about the or-**
28 **ganization of cell types and tissues within this universal cell embedding space, and leveraged**
29 **it to infer function of newly discovered cell types. UCE's embedding space exhibits emergent**
30 **behavior, uncovering new biology that it was never explicitly trained for, such as identifying**
31 **developmental lineages and embedding data from novel species not included in the train-**
32 **ing set. Overall, by enabling a universal representation for every cell state and type, UCE**
33 **provides a valuable tool for analysis, annotation and hypothesis generation as the scale and**
34 **diversity of single cell datasets continues to grow.**

35 Introduction

36 Cells are the fundamental unit of life and biologists have long conceptualized cells as members
37 of different universal landscapes [1–4]. A notable example of this is the Waddington landscape,
38 which presents a theoretical framework for the developmental lineages of cells as they transition
39 from pluripotent stages such as stem cells to more terminally differentiated end points [5]. Broadly,
40 the field of cell biology has sought to map the range of phenotypes that cells might exhibit, their
41 interrelationships, and the shifts between these states during development and disease [6–10].

42 The substantial growth in the size of single-cell RNA sequencing (scRNA-seq) datasets
43 presents a fresh opportunity to revisit these questions. Detailed transcriptomic snapshots of cells
44 are now widely available from a range of timepoints, tissues, donors, and species [11–13]. These
45 rich, high-dimensional states are typically distilled into low-dimensional vectors or embeddings
46 to facilitate computational analysis [14, 15]. However, existing computational approaches strug-
47 gle to jointly analyze these diverse datasets. The unified representations they produce are often
48 unable to extend to new datasets due to species-specific constraints in their construction or the
49 presence of dataset-specific artifacts (or batch effects) which can obscure the underlying biologi-
50 cal signal [16, 17].

51 Some computational methods for scRNA-seq data have managed to overcome these limita-
52 tions, but at the cost of requiring model tuning for each new dataset, thus rendering the represen-
53 tations non-universal [15, 18, 19]. As a result, whenever a new experiment is performed and new
54 data is collected, it requires dedicated, resource-intensive data labeling and model training to per-
55 form even the most standard analyses, such as clustering or annotation. This process is both time
56 consuming and inefficient, and results in sub-optimal analyses based on small, limited and private
57 datasets.

58 Recent advances in the field of artificial intelligence have enabled general-purpose founda-
59 tion models (such as ChatGPT [20, 21], PaLM [22], Llama [23] and SAM [24]) that can learn
60 universal representations that are then applied to diverse downstream tasks and analyses. These
61 foundation models are not specifically trained for these downstream tasks, thus presenting clear
62 instances of emergent capabilities [25]. This foundation model strategy has also found valu-
63 able applications in biological contexts such as learning representations of protein and DNA se-
64 quences [26, 27]. While some recent work has applied foundation model architectures to single-cell
65 genomics data, the unique characteristics of these datasets necessitate a specialized modeling ap-
66 proach to fully realize their potential [28, 29]. Directly modeling gene expression as text in the

67 form of a sequence of genes is both inefficient from a learning perspective and often relies on
68 inaccurate biological assumptions.

69 Here, we present Universal Cell Embedding (UCE), a foundation model for single-cell gene
70 expression that is designed to address questions in cell and molecular biology. UCE is uniquely
71 able to generate representations of new single-cell gene expression datasets with no model fine-
72 tuning or retraining while still remaining robust to dataset and batch-specific artifacts. Moreover,
73 it does so while requiring no cell type annotation and no input dataset preprocessing, such as
74 gene selection. UCE can be applied to any set of protein-coding genes from any species, even
75 if they are not homologs of genes seen during training. UCE learns a universal representation of
76 cell biology that is intrinsically meaningful and can extend insights beyond the data that has been
77 experimentally observed. The representations learned by UCE display an emergent organization of
78 cell types that is consistent with known biology. These cell embeddings can be used to accurately
79 predict cell types with no additional model retraining, showing improved performance in dataset
80 integration against existing atlas-scale integration methods.

81 UCE presents a novel approach to analyzing cell states. It enables the mapping of new
82 data into a universal embedding space, already populated with annotated reference states. This
83 strategy addresses issues such as noisy measurements that limit data alignment across different
84 experiments, and reduces reliance on small sets of marker genes to translate insights across studies
85 [30]. UCE empowers researchers to utilize existing models on new data without needing data
86 labeling or model retraining. This can foster novel cross-dataset discoveries and overcome the
87 limitations currently faced when working with small, isolated datasets. For instance, a cell type
88 classifier trained to predict specific immune cell types can be seamlessly applied to a completely
89 new dataset. Thus, UCE offers a versatile, efficient, and broadly applicable framework for the
90 analysis of cell states.

91 **Results**

92 **A biologically-informed foundation model for single cell gene expression.**

93 Integrating single-cell RNA sequencing (scRNA-seq) datasets is challenging for two primary
94 reasons: scRNA-seq data does not always contain the same genes, or features, and those features
95 are plagued by dataset-specific experimental artifacts or batch effects, which means models have to
96 be built separately for each dataset. UCE overcomes these challenges by abstracting cells as ‘bags

97 of RNA' [31]. UCE (Fig. 1a) converts the RNA gene expression of a single cell into an expression
98 weighted sample of its corresponding genes. Next, UCE represents the sample's genes by their
99 protein products, using a large protein language model. This allows UCE to meaningfully represent
100 any protein-coding gene, from any species based on sequence alone, regardless of whether the
101 species had appeared in the training data. Finally, after incorporating additional metadata about
102 genes' chromosomal locations, this representation is fed into a large transformer model [32]. UCE
103 is able to map any cell, from any tissue, or any species, into one shared universal space, with no
104 additional training.

105 In particular, UCE takes as an input (1) scRNA-seq count data and (2) the corresponding
106 protein embeddings, generated by a large protein language model, ESM2 [33], for the genes in the
107 dataset. The ESM2 protein language model takes amino acid sequences as an input and produces
108 a numerical representation called a protein embedding. Given the expression count data for a cell,
109 UCE takes a weighted and normalized sample, with replacement, of the cell's genes. This sample
110 can only contain genes which had non-zero expression, and can contain multiple copies of each
111 gene. These genes are then tokenized by converting them to the protein embedding representation
112 of the protein that they code for [34]. Genes belonging to the same chromosome are grouped
113 together by placing them in between special tokens and are then sorted by genomic location. A
114 special token representing the entire cell, the 'CLS' token, is appended to the beginning of the cell
115 representation [35]. This combined representation is passed into a transformer neural network. The
116 embedding of a cell is taken as the embedding of the CLS token at the final layer of the transformer
117 (Fig. 1a).

118 UCE is trained in a completely self-supervised manner, and thus does not make use of any
119 cell type or dataset-based annotations. Although including cell type annotations in model archi-
120 tecture or training might seem like a compelling design choice, cell type labels may contain inac-
121 curacies or biases, and including these labels can distort the structure of embedding spaces [36].
122 Ultimately, it would be preferable if the organization of cells within a model were to emerge natu-
123 rally, rather than relying on human labeling.

124 To train the UCE model, a random subset (20%) of genes that were expressed are masked
125 before sampling. These expressed genes are combined with a random subset of genes which had
126 zero expression (non-expressed genes) to form a set of query genes. Each of these query genes'
127 protein embedding tokens is combined with the UCE embedding of the cell they were generated
128 from, and this joint embedding is passed into a fully connected neural network that predicts if that

129 gene was expressed.

130 UCE is a 33 layer model consisting of over 650 million parameters. UCE was trained across
131 more than 300 datasets that are largely collected from the CellXGene corpus [37] consisting of
132 over 36 million cells, for 40 days across 24 A100 80GB GPUs (Methods, Extended Data Table
133 2, Supplementary Table 2). The model's weights and implementation are freely available and the
134 model will be hosted as an openly available resource for the research community to run inference
135 on new datasets.

136 **UCE creates an Integrated Mega-scale Atlas (IMA) of 36 million cells.**

137 We apply UCE to generate an Integrated Mega-scale Atlas (IMA) of 36 million cells sam-
138 pled from diverse biological conditions, demonstrating the emergent organization of UCE cell
139 representations (Fig. 1b). We find that cells within the UCE space naturally cluster by biological
140 conditions like cell type, while mixing among experimental conditions like batch (Fig. 1b). Since
141 UCE is trained in a self-supervised manner, this organization represents an emergent behavior of
142 the model. The IMA contains numerous cell type alignments, across tissues and species.

143 To investigate the emergent organization of the IMA, we inspect how tissue residency can
144 influence the state of cell types. Although macrophages found in different tissues are characterized
145 by diverse transcriptional identities [38], they align closely in the UCE space (Extended Data Table
146 1). For the purpose of our analysis below, we first determine the central location of each cell type
147 and tissue combination in the IMA space, by averaging the UCE embeddings of the cells from that
148 combination, creating a tissue and cell type 'centroid'.

149 Cells in the IMA have been pre-labeled by their cell type. As these labels were never used
150 for training the UCE model, we use them to validate the quality of the learned representation.

151 For example, in the IMA, human macrophages are found in 73 different tissues and among these
152 tissues, 72% (53) of tissue-specific macrophage centroids were embedded closest to a macrophage
153 centroid from another tissue. Considering the 3 nearest centroids increases this percentage to 93%
154 (Extended Data Table 1). Similar cross-tissue homogeneity can also be identified in other prolific
155 cell types, like endothelial cells or neurons. This demonstrates that UCE, without any explicit
156 training or labels, identifies that macrophages have a unique cellular identity that is shared across
157 tissues. More broadly, it is an example of UCE's emergent organization that is consistent with
158 known biology even though not explicitly trained for.

159 **UCE embeds new datasets without additional model training.**

160 We evaluated the universality of UCE representations by directly mapping new datasets
161 which were not part of the training set into the embedding, without any additional training or
162 refinement of the UCE model. This is referred to as a 'zero-shot' capability, since the model was
163 never trained on any samples from the new dataset (Fig. 2a). Performance in a zero-shot setting
164 demonstrates a novel and valuable capability, and is necessary to achieve universality. When a
165 model's weights are updated, such as during fine-tuning, its underlying structure changes, and it
166 may overfit to whatever data it is trained on. Because this underlying structure changes, the rep-
167 resentations the model learns for data are no longer universal. While a variety of deep learning
168 models have been proposed for this cell embedding task, we choose to compare the performance
169 of UCE to other self-supervised transformer-based methods. This is because they do not rely on
170 cell type annotation, are trained on large datasets, have high model capacity, and can be run in a
171 zero-shot setting. In particular, we compare against Geneformer [28] and scGPT [29]. Geneformer
172 represents cells as lists of genes sorted by their expression, while scGPT represents cells as lists of

173 genes with binned expression values.

174 We assess the performance of these methods on a completely new and yet unreleased dataset
175 (as of the publication of this manuscript), Tabula Sapiens v2, which contains diverse human data
176 from 581,430 cells, 27 tissues, 167 batches and 162 unique cell types. Tabula Sapiens is collected
177 in a highly standardized way and represents one of the largest ‘gold-standard’ expert annotated
178 datasets available. We use established metrics for embedding quality that measure the conservation
179 of cell type information and the correction of batch effects (Methods). We compared several meth-
180 ods and found that UCE substantially outperforms the next best method Geneformer by 13.9%
181 on overall score, 16.2% on biological conservation score, and 10.1% on batch correction score
182 (Supplementary Table 1). To comprehensively assess the value of these zero-shot embeddings, we
183 also compare UCE to fine-tuned methods that are conventionally used for this task. Notably, UCE
184 even performs slightly better than non-zero-shot methods that require dataset-specific training:
185 scVI [15] and scArches [18].

186 Tabula Sapiens v2 includes cells measured using both droplet or plate-based sequencing
187 methods. Correcting technology-based batch effects, even for fine-tuned models, can be difficult.
188 UCE zero-shot embeddings of the Tabula Sapiens v2 Ovary tissue, which contains 45,757 cells
189 profiled using 10x-primev3, and 3,610 cells profiled using Smart-seq3, successfully corrects batch
190 effects at the same level as fine tuned methods, while more accurately representing cell types.
191 When scored using the single cell integration benchmark (SCIB), UCE’s batch correction scores
192 are close to that of scVI and scArches, while its bio conservation scores are higher (Supplementary
193 Table 4).

194 For all cell types in Tabula Sapiens v2, we calculate the silhouette width score of each zero-

195 shot embedding method. For 67% of cell types, UCE has the highest silhouette score of any
196 method (Extended Data Table 8). UCE outperforms Geneformer on 80% of cell types, tGPT
197 on 73% of cell types, and scGPT on 83% of cell types. Notably, UCE accurately embeds B
198 cells, while Geneformer and scGPT fail to do so (Supplementary Fig. 2a). In Tabula Sapiens
199 v2, the silhouette width score of B cells is 93% higher in UCE versus scGPT and 25% higher
200 versus Geneformer. Additionally, B cells within the UCE embedding space can be accurately
201 mapped to an existing reference. We train a simple logistic classifier on the UCE embeddings of
202 the Immune Cell Atlas [39], and then apply the classifier to B cell embeddings from Tabula Sapiens
203 v2. This classifier accurately classifies the Tabula Sapiens v2 cells as memory and naive B cells
204 (Supplementary Fig. 2b), which is confirmed with marker gene analysis (Supplementary Fig. 2c).

205 To further compare the performance of UCE and other foundation model approaches, we
206 evaluate embedding quality on a complex dataset featuring 382 cell type clusters, the Human Brain
207 Atlas [12]. UCE outperforms Geneformer and scGPT, and can be used to further investigate di-
208 verse cell types, like “Splatter neurons”, by comparing them to the IMA (Supplementary Note
209 6). Overall, these results illustrate that UCE has the unique capability to meaningfully integrate
210 new, previously unseen datasets into a universal cell representation space with no additional model
211 training.

212 **UCE embeds diverse cell types from organisms that were not part of the training data.**

213 UCE is also able to align datasets from novel species without additional model training. This
214 is due to the fact that UCE is not dependent on any particular genome—each gene of interest is
215 translated to a corresponding protein sequence, which is then embedded in a universal protein
216 space. The representation in this space is independent of species and importantly does not require

217 any judgment about whether particular pairs of genes are homologs or not. Since UCE can analyze
218 cell atlas data from distinct species that were not part of the training set, the extent to which it
219 succeeds in this task is a stringent test of whether UCE displays emergent behavior.

220 UCE's training data is composed of datasets from eight species: human, mouse, mouse
221 lemur, zebrafish, pig, rhesus macaque, crab eating macaque and western clawed frog. We apply
222 UCE to embed datasets from three novel species that were not included in the training set. For each
223 species, we generate a zero-shot embedding and then determine the nearest cell type centroid from
224 the IMA for each of the dataset's existing annotated cell types. For all three species we observed
225 very high agreement between independent annotations of the novel species' data and the nearest
226 cell type centroids in the IMA.

227 Within a dataset of green monkey lymph node and lung cells [40], for 13 of the 17 cell
228 type centroids, the closest centroid from another species corresponds to the same cell type in the
229 green monkey. This match extends to all 17 centroids when considering the three nearest centroids
230 (Extended Data Table 1, Fig. 2c, 2d). Moreover, a population of lymph node cells that were
231 originally labelled as B cells, form a distinct cluster in UCE space (Supplementary Fig. 3b).
232 Differential expression analysis revealed that this cluster predominantly expresses a T cell marker,
233 *Cd3d* (Supplementary Fig. 3a, 3c).

234 In the case of naked mole rat spleen and circulating immune cells [41], for 17 out of 24 cell
235 types, the nearest cross species centroid matches the naked mole rat cell type (Extended Data Table
236 1, Supplementary Fig. 4b). In the case of chicken, we embed two distinct chicken datasets, chick
237 retina [42] and developing chick heart [43] (Supplementary Fig. 5a, 5b). Different eye-specific
238 neurons within the chick retina map to mouse lemur neurons, such as chick oligodendrocytes,

239 which are closest to mouse lemur oligodendrocytes (Extended Data Table 1). In chicken heart,
240 12 of 15 cell type centroids are matched within the nearest two cross species centroids (Extended
241 Data Table 1). No bird species were included when training UCE.

242 We compare UCE's performance to a state-of-the-art method for cross-species label transfer,
243 SATURN [34]. For each of the four datasets, we integrate them with a paired human dataset
244 from the same tissue from Tabula Sapiens v1, except for chicken retina, which was paired with
245 retina data from Orozvo et al [44]. In comparison to UCE, which is zero-shot and unsupervised,
246 SATURN is a fine-tuned method and weakly-supervised: it is aware of each species' cell type
247 annotations individually. Still, UCE outperforms SATURN for cell type label transfer between the
248 human and the new species for three out of four datasets, chicken heart, chicken retina and naked
249 mole rat spleen (Supplementary Note 5).

250 While UCE successfully integrates data from these new species, it still has limitations when
251 assessing species that are more evolutionarily distant from the species in the training data. We
252 create a zero-shot embedding of Tabula Drosophilae [45], a large multi-tissue fly cell atlas, and
253 evaluate UCE's performance by transferring labels from Tabula Sapiens v1 and v2 to the fly cell
254 atlas using cell type centroids. Predicted fly cell types are inaccurate using this method: many fly
255 cells are incorrectly annotated as fat cells, including adult epithelial cells, adult muscle cells and
256 adult trachea cells. Additionally, other adult muscle and epithelial cells are incorrectly annotated
257 as leukocytes (Extended Data Table 4).

258 Altogether, these results highlight that UCE can be directly applied to investigate new and
259 diverse datasets from previously unobserved species. While model performance does not neces-
260 sarily extend to very distant species, such as fly, inclusion of more species from across the tree of

261 life could help solve this issue; both by improving models' performance as well as by providing a
262 more appropriate reference to compare data to.

263 **UCE learns a meaningful organization of cell types in previously unseen data.**

264 Moving beyond metrics focused on individual cell type clusters, we also examined the struc-
265 ture of the universal embedding space as a whole, through the relative positioning of different cells
266 within it. A meaningful arrangement of cell types emerges upon embedding all the cells from the
267 Tabula Sapiens v2 dataset from the lung tissue (Fig. 3a). Not only do distinct cell types like T cells,
268 monocytes and endothelial cells cluster together, but higher-level categories, such as immune cells
269 and epithelial cells, are also clearly distinguished. When compared to the cell hierarchy derived
270 using the Cell Ontology [46], UCE identified clusters showed higher similarity (as measured using
271 Adjusted Rand Index) than other zero-shot embedding methods (Supplementary Fig. X).

272 To further assess the organization of all cells within the embedding, we compared distances
273 between pairs of cell types across all tissues in the embedding space to their distances in the Cell
274 Ontology tree (Fig. 3b). We hypothesized that cells that are known to be similar based on the
275 cell ontology would likely also be closer together in the embedding space, and that the degree of
276 closeness would be correlated with ontological similarity. The results validate this relationship: at
277 each additional unit of separation between cell types in the cell ontology tree, there is a significant
278 increase in the embedding distance in UCE between those cell types. We consistently observed
279 this trend up to a distance of 5 hops in the ontology tree (Fig. 3b). However, beyond that, the effect
280 levels off (Supplementary Fig. 6). This is expected due to the curse of dimensionality in high-
281 dimensional spaces and the variability in the level of ontological refinement in different branches
282 of the ontology (Supplementary Note 3).

283 We also noted significant colocalization among cells originating from the same developmen-
284 tal lineages, in particular from the mesoderm, endoderm, and ectoderm germ layers. For Tabula
285 Sapiens v2, 90 out of 97 of the centroids for mesoderm-derived cell types had other mesoderm-
286 derived cell type centroids as their closest neighbors. A similar pattern was observed for 46 of the
287 56 endoderm-derived cell types and 22 of the 30 ectoderm-derived cell types (Supplementary Fig.
288 7a). A neural network classifier trained to predict the germ layer of origin for individual held-out
289 cell types using their universal embeddings showed an accuracy of over 80% (Supplementary Fig.
290 7b). When mapping unseen data from the bone marrow, we observe a clustering of cell types that
291 aligns well with both developmental stage—where early progenitors are closer to each other in
292 the embedding space—and lineage, with more developed cell types in the lymphoid and myeloid
293 lineages clustering distinctly. (Supplementary Figure 16)

294 The accuracy of cell type organization in the Tabula Sapiens v2 lung dataset was evaluated
295 by comparing it with other lung datasets in the IMA (Fig. 3c, Supplementary Fig. 8). Four dif-
296 ferent endothelial cell subtypes are observed to map correctly to their corresponding counterparts
297 in the IMA. Similarly, lung ciliated cells correctly map to their counterpart in the larger corpus
298 despite the presence of four different ciliated cell subtypes (Fig. 3c). Further analysis of the align-
299 ment of cell type centroids between Tabula Sapiens v2 and the IMA across all tissues showed
300 an exact alignment for 41% of cell types (Methods). This alignment, based on the three nearest
301 neighbor cell type centroids, is 65% more accurate compared to that measured in the original gene
302 expression space (Fig. 3d). When focusing on the single nearest centroid, the alignment accuracy
303 improves by 92%. Many inexact matches are caused by differences in the labeling resolution of
304 different datasets in the IMA (Supplementary Tables 5, 6, Extended Data Table 9). These results

305 demonstrate that UCE can effectively learn a universal representation of cell biology that not only
306 enables discrimination between individual cell types but also captures their relative similarities
307 across scales with the potential to reveal deeper insights into development and function.

308 **A workflow for decoding the function of newly discovered cell types.**

309 UCE's zero-shot embedding capabilities unlock novel computational analyses of scRNA-
310 seq data and aid in hypothesis generation. Beyond identifying novel cell type clusters, UCE differs
311 from other methods in that the same cell type can also be easily compared against all previously
312 assayed cells across tissues, disease states and species. Moreover, UCE is not biased in this process
313 by existing annotations, opening the door for discovery of novel function (Fig. 4a). With existing
314 fine tuning based methods, every searched dataset would need to be integrated, requiring repeated
315 model retraining. Thus, UCE enables a new workflow for scRNA-seq data analysis that performs
316 an unbiased search across the universe of cell biology.

317 We present an example of this analysis by using the recently identified kidney Norn cell as
318 a case study. The kidney Norn cell is the long-sought erythropoietin (*Epo*) producing cell in the
319 kidney, and is characterized as fibroblast-like. We perform a zero-shot embedding of mouse renal
320 cells from [47], which produces a cluster of cells corresponding to Norn cells (Fig. 4b).

321 Using a simple logistic classifier trained on the embedding of mouse renal cells, we predict
322 the existence of Norn cell clusters in many kidney datasets. Since this classifier takes universal cell
323 embeddings as an input, we can directly apply it to all 36 million cells in the IMA, in a manner
324 unbiased by cell type annotations ascribed by previous studies. To evaluate the model's predictions
325 that these are Norn, or Norn-like cells, we investigate the expression of canonical Norn cell marker
326 genes. Cells classified as Norn cells in the top 13 kidney datasets by Norn abundancy demonstrate

327 preferential expression of the Norn markers *Dcn*, *Lpar1*, *Coll1a1*, *Cxcl12*, and *Cfh* (Extended Data
328 Table 3). Notably, *Epo* transcripts, which are often missing from datasets and lowly expressed, are
329 not typically differentially expressed in these cells. *Epo* cannot readily be used as a marker gene
330 for Norn cells because of a variety of factors, including low overall expression, even in hypoxic
331 Norn cells, the bursty nature of *Epo* transcription, and the fast degradation of *Epo* messenger
332 RNA upon reoxygenation [47]. *Cxcl14*, another marker of Norn cells, displays mixed expression
333 patterns in these predicted Norn cells (Fig. 4c). The same pattern of marker gene expression is
334 also found in cells from other tissues, including lung and heart datasets (Fig. 4c). Additionally,
335 these predicted cells also share a common set of genes that are lowly expressed in mouse renal
336 Norn cells (Supplementary Fig. 9). The tissues with the highest number of predicted Norn cells
337 were gonad, heart and lung. Finally, we also identify differences in gene expression specific to
338 each tissue (Supplementary Figure 10). While *Epo* expression has been previously observed in
339 the heart and lung tissue, the mechanisms and cell types associated with this expression, and their
340 relation to kidney Norn cells have not been previously determined [48]. Overall, this demonstrates
341 that UCE can serve as an unbiased tool for predicting novel similarities between cells.

342 **UCE helps interrogate alternate lung disease outcomes.**

343 Lastly, we apply UCE and our simple Norn cell classifier to investigate Norn-like cells in lung
344 diseases. We generate an embedding of lung cells sampled from patients with idiopathic pulmonary
345 fibrosis (IPF), chronic obstructive pulmonary disease (COPD), or patients from a control group
346 [49]. We identify Norn-like lung cells that preferentially express Norn markers in all three groups
347 (Fig. 4d).

348 For these Norn-like lung cells, we identify differences across disease groups (Fig. 4e). COPD

349 and IPF are both associated with elevated bloodstream *Epo*, but COPD has levels higher than
350 IPF. Additionally, in patients with IPF, secondary erythrocytosis is absent or reduced compared
351 to patients with COPD [50–52]. Given the identification of Norn-like cells in the lung, and Norn
352 cell’s production of *Epo*, it is possible that this difference in disease prognosis could be related to
353 disease associated differences in Norn-like cells.

354 COPD predicted Norn-like cells express genes (*Lum*, *Crispld2*) involved in glycosaminogly-
355 can pathways at higher levels than IPF or control predicted Norn-like cells [53,54]. Norn-like cells
356 in both COPD and IPF express *Gpx3* and *Igfbp6* at significantly lower rates than the control group
357 (Figure 4d, Extended Data Table 7).

358 Taken as a whole, these results indicate that cells with similar transcriptional states to Norn
359 cells can be found in other tissues in the body, and such cells may play a previously undescribed
360 role in disease. UCE greatly facilitates an analysis of this scale and diversity because it is a univer-
361 sal model that is agnostic to tissue, species or disease state. In order to ground this analysis, results
362 are confirmed using expression of canonical marker genes. However, as universal analyses become
363 more complex, it is possible that such assessments might be made based solely on the predictions
364 of foundation models.

365 Discussion

366 UCE is a single-cell foundation model that is built from the ground up to represent cell biology
367 across the wide array of single-cell datasets. We envision UCE as an embedding approach that
368 enables researchers to map any new data, including entire atlases, into an accurate, meaningful and
369 universal space. The embedding space that emerges from UCE is highly structured and diverse and
370 aligns cell types across tissues and species. Additionally, these cell types organize themselves in a

371 pattern that reflects existing biological knowledge.

372 The UCE model has broad implications for the creation of large foundation models for single
373 cell biology. For large foundation models to be truly useful for scientific discovery, they must have
374 unique qualities that distinguish them from existing methods. Zero-shot embeddings are one such
375 important capability because it enables an intrinsically meaningful representation that can extend
376 insights beyond the data that has already been observed and annotated experimentally. Our results
377 demonstrate that UCE can achieve such a generalizable representation across different datasets
378 while maintaining accuracy on individual datasets, comparable to methods that require retraining
379 for each specific dataset. To ensure that UCE’s embeddings, or any downstream models trained on
380 them, remain universally shareable, we have designed UCE to be used as-is, without any model
381 fine-tuning. This allows UCE representations to serve as a universal way of connecting any single-
382 cell gene expression dataset.

383 By building UCE, we enable novel analyses of scRNA-seq data. In order to establish the uni-
384 versality and accuracy of UCE, we perform a number of different benchmarks, mainly focused on
385 correctly identifying and matching expert-annotated cell types. However, these analyses are still
386 far from perfect, as they are generally limited by the resolution of cell type labels. To better under-
387 stand single-cell foundation models, and especially how they scale, new analyses and benchmarks
388 that surpass this resolution limit should be developed. Such benchmarks could focus on measuring
389 a model’s ability to encode response to perturbation or to integrate data from different modali-
390 ties. Because of their “black box” natures, foundation models for biology represent a further step
391 away from explainable predictions. In addition to benchmarks, which can point to what models
392 performs the best, new interpretability tools must be developed to explain why these models make

393 their predictions [55–58].

394 UCE establishes a framework in which physical scales of biology, learned by large machine
395 learning models, are directly connected. In this framework, molecular representations, embeddings
396 of proteins based on sequence, are aggregated and used to construct representations of cells. Such
397 an approach maximizes generalizability and the scope of genomic data that models can be trained
398 on. Since these scales are connected, improvements in modeling in one scale can help improve
399 results in the next. For example, by creating a model which could jointly represent molecules like
400 proteins, RNA and DNA, one could enable a new cell based model to encode additional complex
401 features, e.g. non-coding RNAs, regulatory DNA, alternative splicing, RNA velocity etc. Finally,
402 current scRNA-seq foundation models, including UCE, do not account for any information con-
403 tained in the raw RNA transcripts. By aligning these transcripts to the reference genome, vital
404 data on genetic variation and crucial RNA-splicing processes are discarded [59]. As these models
405 adopt more biologically-relevant features, they will increasingly be able to simulate the biological
406 processes of cells, leading to the creation of “Virtual Cells”.

407 In 2002, Nobel laureate Sydney Brenner identified many of the core motivations for the
408 creation of cell atlases and virtual cells. Virtual cells should be the goal of biological foundation
409 modeling, because cells are the “real units of function and structure in an organism” [60]. Brenner
410 also identified the need for such models to be computationally efficient, predictive, and able to
411 generate new cell types. We believe that UCE represents a significant advancement in the progress
412 towards a virtual cell. Through learning a universal representation of every cell state and type, we
413 expect that UCE will be a valuable tool for analysis, annotation and hypothesis generation as the
414 scale and diversity of single-cell datasets continues to grow.

415 **Methods**

416 **Overview of UCE.**

417 UCE (Universal Cell Embedding) is a machine learning model for mapping single-cell gene
418 expression profiles into a universal embedding space, denoted as \mathcal{U} . In this space, each cell c_i is
419 represented as a d_{emb} -dimensional vector, where $d_{emb} = 1280$.

420 The model takes as input a dataset \mathcal{D} with N cells $\{c_i\}_{i=1}^N$. Cells in \mathcal{D} can be drawn from
421 one or more distinct scRNA-seq experiments. Each cell c_i in \mathcal{D} is described by a gene expression
422 vector $\mathbf{x}^i \in \mathbb{N}^{K_i}$, where K_i is the number of genes measured in c_i and can differ across \mathcal{D} . The gene
423 expression vectors $\mathbf{x}^i \in \mathbb{N}^{K_i}$ are not subset to those with high variance. UCE defines a function
424 $f_u : \{\mathbb{N}^{K_i} \rightarrow \mathbb{R}^{d_{emb}}\}_{i=1}^N$ that maps each gene expression vector \mathbf{x}^i to its cell embedding vector \mathbf{h}^i .

425 **Model input: Gene representation.**

426 The expression of gene g in cell c_i is denoted by x_g^i , where g represents any protein-coding
427 gene. The corresponding token embedding p_g is a pretrained embedding for the protein(s) encoded
428 by the gene g . These embeddings are derived from a pretrained protein language model that takes
429 an amino acid sequence as input and returns a d_p -dimensional embedding vector as output. To
430 create p_g , we take the average of all proteins coded by gene g . In the context of UCE, we can
431 formulate this as a dictionary that maps each gene g to a d_p -dimensional protein embedding vector.
432 Specifically, we employ the ESM2 model, which yields embeddings of size $d_p = 5120$ [33, 34].

433 Protein language models are chosen for gene representation because they can generate uni-
434 versal representations of any protein sequence. Therefore, for new species, all that is required is
435 to have the amino acid sequence of that species' protein coding genes. These genes do not need
436 to have solved structures and orthology does not need to be calculated between them and the ex-

437 isting training data. Model training ablations demonstrate that among a class of different protein
438 language models, UCE models trained with ESM2-15B performed the best (Supplementary Note
439 4, Supplementary Table 3).

440 **Model input: Cell representation.**

441 For each cell c_i in the input dataset \mathcal{D} , we identify two distinct sets of protein-coding genes:
442 the expressed genes G_i^+ and the non-expressed genes G_i^- . These sets are defined as follows:

$$G_i^+ = \{g \mid x_g^i > 0\} \quad (1)$$

$$G_i^- = \{g \mid x_g^i = 0\} \quad (2)$$

443 For producing the cell embedding, a multi-set of 1024 non-unique genes G_i^s are sampled
444 from the expressed genes G_i^+ , with replacement. The probability of sampling a gene $g \in G_i^+$ is
445 weighted by the log normalized expression of that gene, which can be formulated as:

$$P(g \mid c_i) = \frac{\log(x_g^i + 1)}{\sum_{g \in G_i^+} \log(x_g^i + 1)} \quad (3)$$

446 where x_g^i is the expression count of gene g in cell c_i , and the sum in the denominator is over
447 all genes in G_i^+ .

448 Once the multi-set G_i^s is compiled for each cell c_i , we arrange the genes within each chro-
449 mosome according to their genomic positions. Different chromosomes are specified using special
450 chromosome start and end tokens. Start tokens are unique to each chromosome and species. Every
451 chromosome group is combined into a single sequence, with chromosome order randomly deter-
452 mined. A cell-level *CLS* token is appended to the start of the sequence. It is designed to capture

453 the cell-level embedding upon training the model. The final sequence of genes ordered by genomic
454 location and separated by chromosome is referred to as the cell sentence S_i for cell c_i .

455 Ordering the genes using this information appears to have a moderate negative effect on
456 model performance (Supplementary Note 4, Supplementary Table 3). Transformer models do not
457 require any ordering of their inputs, and this metadata was only added to the model in order to
458 enable potential applications, such as examining chromosomal aberrations or synteny between
459 species. Future models of this type may choose to exclude this metadata, or include it using other
460 methods besides positional encodings.

461 **Transformer Architecture.**

462 Each cell sentence S_i is fed into a transformer that consists of n_{lay} layers. Each layer con-
463 tains a multi-head self-attention mechanism with n_{head} attention heads and a feedforward network
464 operating over a hidden space of dimensionality d_{hid} . We also initialize sinusoidally-varying po-
465 sitional embeddings. Gene token embeddings are compressed using a single layer MLP to d_{emb} -
466 dimensional vectors before passing through the transformer.

467 While the transformer architecture is highly performative, it requires significant computa-
468 tional cost to train and evaluate. One important aspect of this cost is the quadratic increase in the
469 runtime of transformers' attention operations proportional to the number of tokens. Such a rela-
470 tionship requires that the number of genes sampled by UCE, 1024, be relatively limited, especially
471 given that individual cells might have more than 1024 uniquely expressed genes. Future model ar-
472 chitectures could explore increasing this context length, or using models with sub-quadratic scaling
473 such as state space models [61]

474 **Model output: Cell embedding.**

475 The final output from the model is the cell embedding vector $\mathbf{h}_{cell}^i \in \mathcal{U}$ which corresponds
476 to the d_{emb} -dimensional embedding of the *CLS* token in the final layer of the model following
477 decoding with an additional MLP.

478 When cells with unrealistic random gene expression patterns, such as those generated by
479 shuffling the expression of real cells, are inputted, the resulting cell embeddings default to a het-
480 erogeneous, out of distribution output (Supplementary Figure 11).

481 **Model training: Cell representation.**

482 At the time of training, we generate a set $G_i^{M+} \subset G_i^+$ by randomly selecting a certain
483 percentage (r_{mask}) of genes from G_i^+ , without replacement. This set is used for computing the loss
484 during training, and is masked from the cell representation.

485 The probability of sampling a gene $g \in G_i^+ \setminus G_i^{M+}$ (Equation 3) is then updated to be:

$$P(g | c_i) = \frac{\log(x_k^i)}{\sum_{g \in G_i^+ \setminus G_i^{M+}} \log(x_j^i)}, \quad (4)$$

486 We also establish two additional gene sets to be used for loss computation: $G_i^{L+} \in G$ and
487 $G_i^{L-} \in G$. G_i^{L+} and G_i^{L-} are randomly selected from the masked set of expressed genes G_i^{M+} and
488 the set of unexpressed genes G_i^- respectively. Both G_i^{L+} and G_i^{L-} are of equal size, specifically
489 $N_{loss}/2$. In the case of G_i^{L-} , the sampling is done without replacement unless $|G_i^-| < N_{loss}/2$.
490 Similarly G_i^{L+} , is also sampled without replacement unless $|G_i^{M+}| < N_{loss}/2$. In this case, G_i^{M+}
491 is used as-is along with additional samples drawn with replacement from the full set of expressed
492 genes G_i^+ .

493 **Model training: Loss Function.**

494 UCE is trained to reconstruct the binarized expression of genes in a cell, when those genes

495 are masked from the model by setting their expression to 0. To calculate the loss function for a
 496 given cell c_i , the cell embedding vector \mathbf{h}_{emb}^i is individually concatenated with every gene g within
 497 both G_i^{L+} and G_i^{L-} . These concatenated vectors then serve as input to a feedforward multilayer
 498 perceptron (MLP), which computes the probability that gene g is expressed within cell c_i .

499 \mathbf{h}_{cell}^i represents the embedding vector for cell c_i and p_g represents the token embedding for
 500 gene g . Then the concatenated vector \mathbf{z}_g^i that serves as input to the MLP for cell c_i and gene g is:

$$p'_g = \text{MLP}(p_g) \quad (5)$$

$$\mathbf{z}_g^i = [\mathbf{h}_{cell}^i || p'_g] \quad (6)$$

501 where $||$ denotes the concatenation operation and p'_g is the compressed protein embedding.

502 The MLP then processes this concatenated input to produce the predicted probability that
 503 gene g is expressed:

$$p(y_g^i) = \text{MLP}(\mathbf{z}_g^i) \quad (7)$$

504 This probability is then used in the binary cross-entropy loss function. The true classification
 505 labels for each gene's expression status in cell c_i are represented by the vector \mathbf{y}^i . UCE is trained
 506 to accurately predict the expression of genes in G_i^{L+} and the lack of expression in G_i^{L-} . The model
 507 is trained using a binary cross-entropy loss, which is averaged across all N_{loss} genes and all N
 508 cells in the minibatch as follows:

$$L = -\frac{1}{N} \sum_{i=1}^N \frac{1}{N_{loss}} \sum_{j=1}^{N_{loss}} [y_j^i \log(p(y_j^i)) + (1 - y_j^i) \log(1 - p(y_j^i))] \quad (8)$$

509 For further details on hyperparameter choices please see Supplementary Table 2. Different
510 hyperparameter choices for this masked loss can impact final model quality. Reducing the masking
511 percentage from 20% to 10% improved model performance, while increasing it to 40% degraded
512 performance (Supplementary Note 4, Supplementary Table 3). In future models, an alternate loss,
513 for example, a generative decoder style loss, could be used, and might improve performance since
514 no genes would be masked during training.

515 **Creating the IMA and dataset preprocessing.**

516 The Integrated Mega-scale Atlas (IMA) used to train UCE was created by combining scRNA-
517 seq datasets from multiple publicly available sources. The majority of IMA data (33.9 million cells
518 and 285 datasets) is human and mouse data downloaded from CZI Cell X Gene (CxG) Census [37]
519 version "2023-07-10" (July 10th, 2023). Duplicate cells were removed by selecting primary cells
520 only. The remainder of the IMA is composed of 2.3 million cells from 28 datasets, from eight
521 different species: human, mouse, zebrafish, rhesus macaque, crab-eating macaque, mouse lemur,
522 frog, and pig.

523 For datasets from the CxG Census, preprocessing only involved filtering cells by minimum
524 gene counts (200) and genes by a minimum cells count of 10. No highly variable gene selection
525 was applied. For datasets collected from other sources, preprocessing was not uniform (Supple-
526 mentary Note 1).

527 For visualization of the IMA (Fig. 1b), predicting green monkey cell types (Fig. 2d), match-
528 ing new species centroids (Extended Data Table 1), and prediction of Norn-like cells (Fig. 4,
529 Supplementary Fig. 9) a representative sample of the IMA was used in place of the full 36 million
530 cells. This representative sample was used in order to speed up computationally intensive tasks like

531 UMAP calculation. The sample was created by randomly choosing 10,000 cells from each dataset,
532 without replacement. For datasets with fewer than 10,000 cells, the entire dataset was included. In
533 total, this representative sample has 2,969,114 cells. The average number of cells per dataset in the
534 sample is 9486. For visualization and centroid calculation, cell types in the sample were coarsened
535 by mapping them to a set of 51 coarse cell types (Extended Data Table 6).

536 **Model Evaluation.**

- 537 • **Zero-shot embedding quality and clustering** For evaluating the quality of embeddings, we
538 used metrics from the single-cell integration benchmark [16].
- 539 • **Cell type organization** For each cell type dendrogram the Euclidean distance was used to
540 perform hierarchical clustering across all cells.
- 541 • **Comparison to cell ontology** Here, we used the tree distance between any two cell types
542 in Cell Ontology [46]. We used the most up to date version of Cell Ontology at the time
543 of writing this paper (Release date: 2024/08/16). To determine the Euclidean distance
544 distribution, we sampled 100,000 random pairs of cells from Tabula Sapiens v2.
- 545 • **Zero-shot cell type alignment to IMA** For each cell type θ , a centroid was identified sepa-
546 rately for data from Tabula Sapiens v2 (TSv2) c_{θ}^T and from IMA c_{θ}^I . For each cell type that
547 is present in both TSv2 and the IMA, the 3 nearest neighbor cell type centroids N_{θ}^T to the
548 centroid in Tabula Sapiens c_{θ}^T were identified. These neighbors could be either from Tabula
549 Sapiens or from the IMA.
550 If this set of neighbors N_{θ}^T to the anchor centroid from TSv2 data c_{θ}^T contains the centroid
551 for the same cell type in IMA data c_{θ}^I , then this was counted as a correct match.

552 This analysis was performed per tissue, both in the UCE embedding space as well as in
553 the original expression space (after log-normalization). In case of the original data rep-
554 resentation, the set of 5704 shared genes across all 184 human datasets in the Integrated
555 Mega-scale Atlas (IMA) were used to represent each cell. The expression counts in each cell
556 are normalized by total counts over all genes, so that every cell has the same total count after
557 normalization. This is followed by a log transformation. This follows standard Scanpy data
558 preprocessing guidelines [62].

559 **Description of other models.**

- 560 • **Geneformer** Geneformer [28] is a transformer based foundation model. Geneformer rep-
561 represents a cell as a list of genes sorted by their expression. Geneformer was trained using
562 masked language modeling, on 30 million cells. For all analyses, the *GF-12L-30M-i2048*
563 model was used.
- 564 • **tGPT** tGPT [63] is a transformer based foundation model. tGPT represents cells, like Gene-
565 former, as a list of genes sorted by expression. However, tGPT is trained as an autoregressive
566 language model, rather than a masked language model. tGPT was trained on 22.3 cells.
- 567 • **scGPT** scGPT [29] is a transformer based foundation model. scGPT represents cells as a
568 list of the expression values of its genes. scGPT is trained to iteratively decode those genes'
569 expressions when some are masked, using generative pretraining. scGPT was trained on 33
570 million cells. For all analyses, the *whole-human* model was used.
- 571 • **scVI** scVI [15] is a variational autoencoder. scVI is trained to reconstruct gene expression
572 values using a zero-inflated negative binomial loss. scVI was used with default parameters

573 for all experiments.

574 • **scArches** scArches builds on top of the scVI architecture to enable transfer learning of cell
575 types. As used in this work, scArches first trains an scVI model on a reference dataset, fine-
576 tunes a cell-type aware scANVI model using the cell types from the reference dataset, and
577 then further finetunes this model on a transfer dataset using architecture surgery. scArches
578 was used with default parameters for all experiments.

579 **Differential expression analysis of predicted Norn cells.**

580 A logistic classifier was trained to predict cell types from UCE embeddings on mouse kidney
581 cells. This classifier was then applied to UCE embeddings from the representative sample of IMA
582 datasets. Datasets were then split by tissue, and the datasets with the most predicted norn cells in
583 each tissue were used for differential expression analysis. The top 13 kidney datasets, top 6 lung
584 and top 6 heart datasets were chosen.

585 For each individual (full) dataset, RNA counts were log normalized, and then differential ex-
586 pression was run using default settings as implemented in Scanpy [62], comparing predicted Norn
587 cells to all other cells in the dataset. The results of these differential expression tests were used
588 to determine the log fold change of marker genes in predicted Norn cells (Fig. 4c, Supplementary
589 Fig. 9).

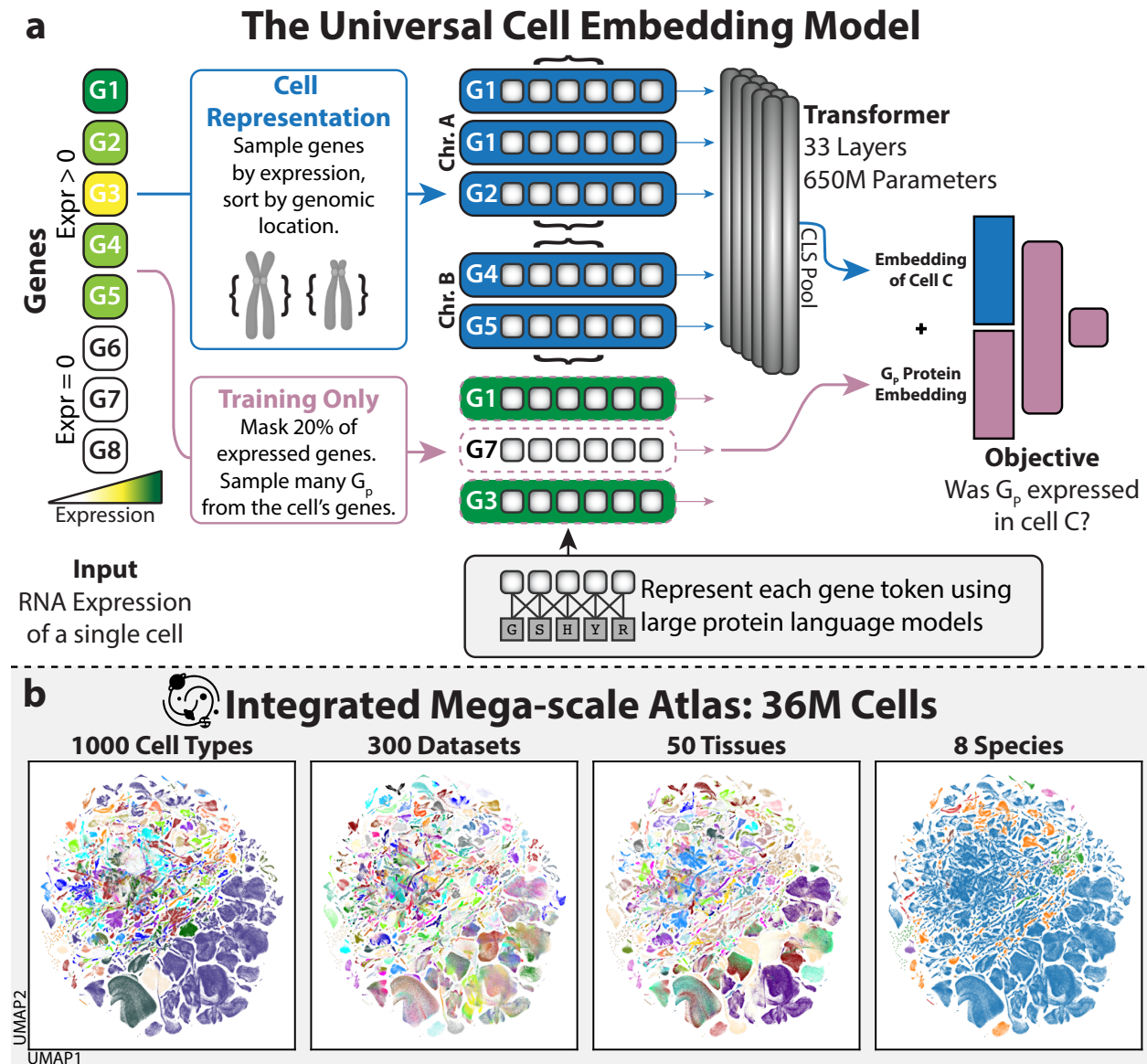


Figure 1: The Universal Cell Embedding Model is a large foundation model for single cell biology (a) Overview of the Universal Cell Embedding (UCE) model. UCE has a unique, biologically motivated representation of cells (blue) and training scheme (purple). Given the gene expression for a single cell, UCE samples with replacement genes that were expressed, weighted by their level of expression. Each gene is represented using a ‘token’ corresponding to its protein product. Gene tokens are represented numerically by using ESM2 protein embeddings, a 15 billion parameter protein language model that takes amino acid sequences as an input. The gene tokens are sorted by genomic location and grouped by chromosome. Chromosome groups are delineated by specific chromosome start tokens and end tokens, joined, and then passed into a transformer neural network. The embedding of the cell is determined by taking the final layer output of a special CLS token that is appended before all the other tokens. To train the UCE model, a portion of genes that were expressed are masked. The model next combines the protein embeddings corresponding to each of these genes with the embedding of the cell, and passes this joint representation through a neural network that predicts if a given gene was expressed in the cell or not. This objective function is then used to update the weights of the model. (b) UMAP visualizations of the universal cell embedding space. We apply UCE to embed 36 million cells, with more than 1,000 uniquely named cell types, from hundreds of datasets, dozens of tissues and eight species, creating an Integrated Mega-scale Atlas (IMA) spanning the universe of cell biology.

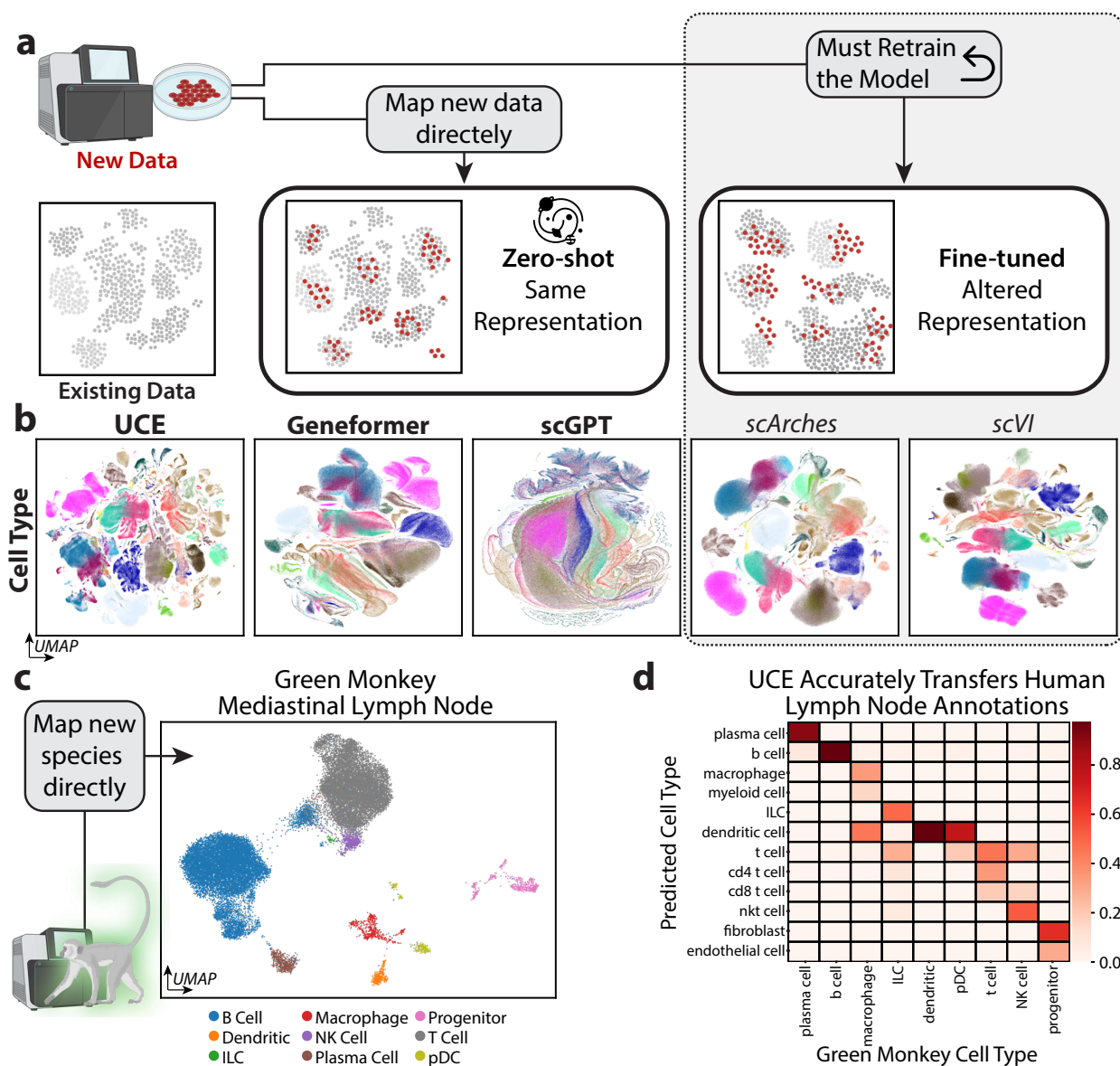


Figure 2: Zero-shot cell embedding capabilities of UCE (a) Comparison of zero-shot and fine-tuned single-cell embedding models. A zero-shot embedding model maps new data directly to the representation space, with no additional model training. In contrast, fine-tuned models must first be retrained on a given dataset, and only then can be applied on that dataset, fundamentally altering the model's representation space. (b) UMAP embeddings of UCE and other methods for Tabula Sapiens v1 and v2, colored by cell type. UCE zero-shot embeddings outperform other methods when scored using metrics from the single cell integration benchmark (Supplementary Table 1) [16]. (c) UMAP of cells from a new species, green monkey colored by cell type. UCE is able to generate high-quality zero-shot embeddings of novel species that were never seen during training. The UCE embedding for green monkey mediastinal lymph node [40] recaptures cell type clusters. Notably, a population of B cells (blue) clusters nearby to T cells, potentially due to expression of *Cd3* (Supplementary Fig. 1). (d) Green monkey lymph node cells can be accurately annotated using the IMA. A logistic classifier is first trained to predict cell types based on UCE embeddings of human lymph node cells. The classifier is then directly applied on green monkey cells to predict the cell types. Predicted cell types have high agreement with the original cell type annotations, demonstrating that UCE can be used to transfer cell type annotations to novel species.

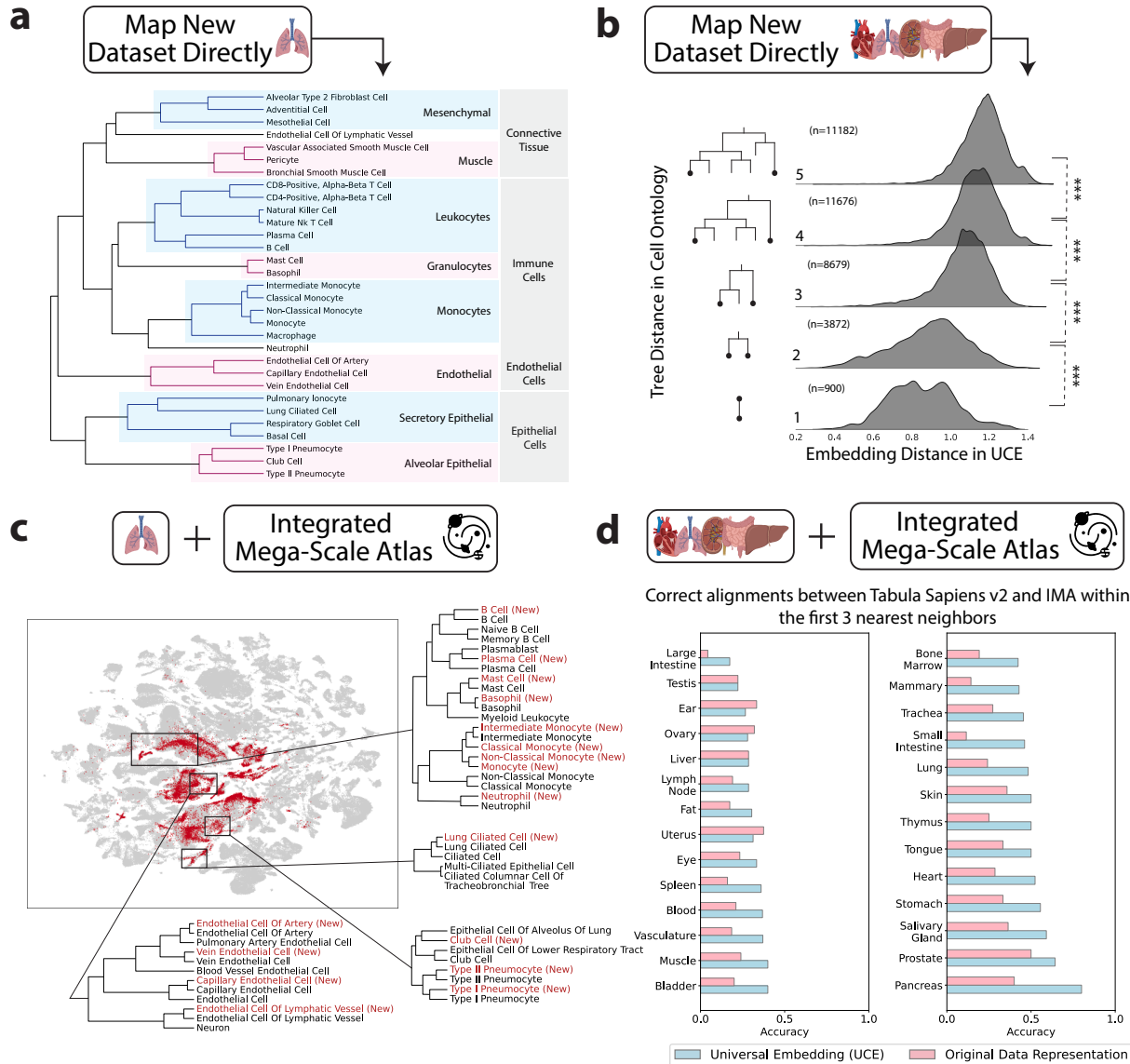


Figure 3: UCE learns meaningful organization of cell types (a) The UCE space generated for new, previously unseen data shows a meaningful arrangement of cell types. Lung data was used from new donors from the Tabula Sapiens Consortium. Dendrogram of hierarchical clustering of all annotated cell types in the UCE embedding space. Closely connected cell types in the dendrogram show meaningful relationships both at finer and coarser scale resolutions. (b) Evaluation of the organization of cell types in the embedding space when compared to Cell Ontology. The x -axis depicts the density of Euclidean distances between all pairs of cells across all tissues for these new donors from the Tabula Sapiens Consortium. The y -axis shows the corresponding tree distance between cell types as found in the Cell Ontology. Stars denote statistical significance, which was established using a one-sided t -test, p values in increasing order of distance: 10^{-106} , 10^{-201} , 10^{-25} , 10^{-131} (c) Mapping data from new donors to the Integrated Mega-scale Atlas (IMA) across multiple lung datasets. Red labels correspond to data from new donors, grey are from IMA datasets. All cell type labels from multiple datasets are displayed as-is, with no modifications or reformatting of text. Accurate alignment between the new dataset and IMA is observed at finer resolution. Four different subtypes of endothelial cells are shown to correctly map to their corresponding counterparts in the complete mega-scale atlas. In the case of lung ciliated cells, they map more closely to their matching counterpart as compared to all other ciliated cell subtypes also present in the IMA. (d) Quantification of cell type alignment between new dataset and IMA. Accuracy in 3-nearest centroid matches between new dataset and IMA cell types at the finest level of original annotation. Results are measured across all 27 tissues in Tabula Sapiens v2 for both the UCE space and the original gene expression space. Tissues are ordered by accuracy in the UCE space.

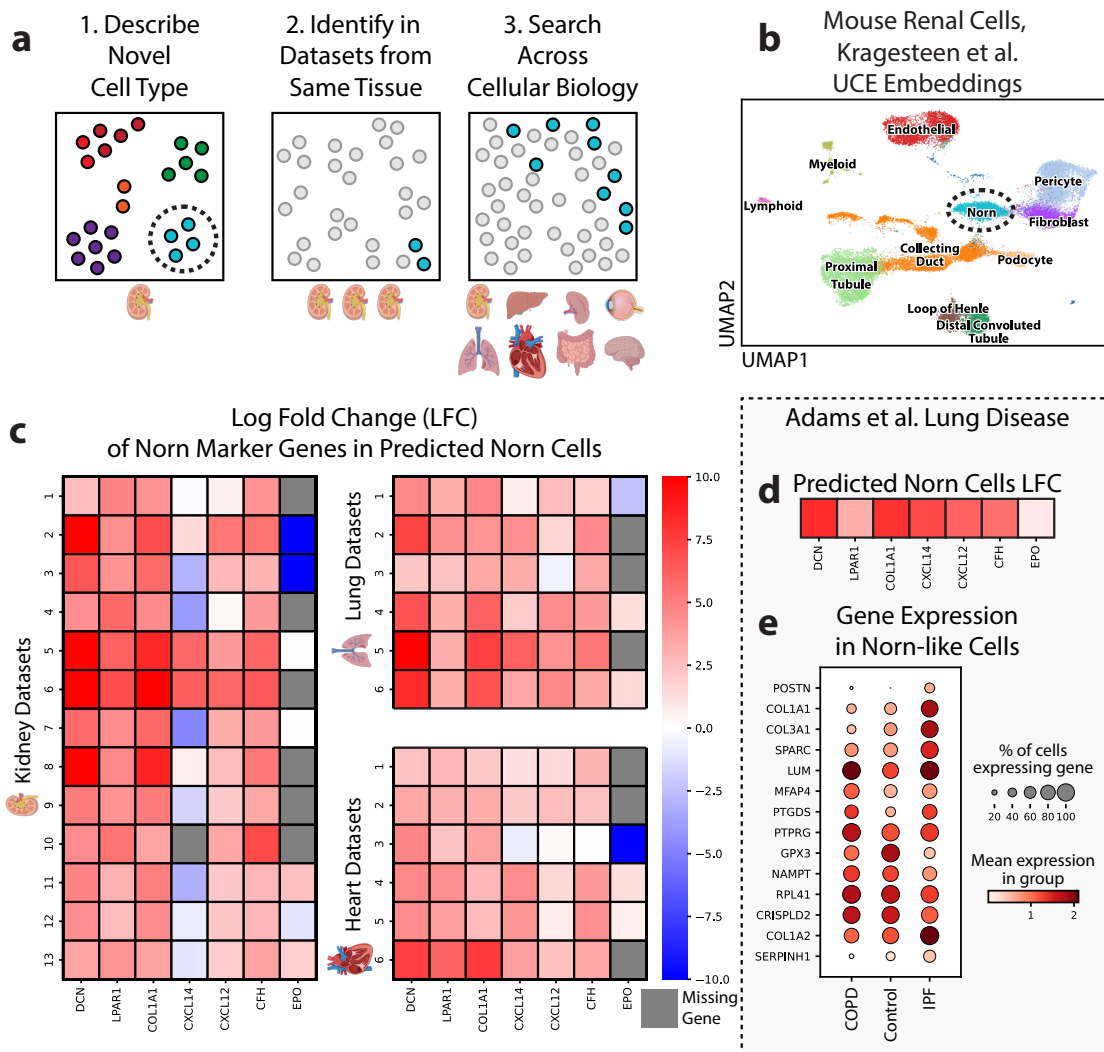


Figure 4: Norn Cell Case Study: UCE unlocks new analyses of single cell datasets (a) Overview of a novel single cell analysis workflow that UCE facilitates. Analysis begins with (1) the identification of a novel cell type (circled) within the embedding space, using methods such as clustering and confirmation using marker gene analysis. (2) Next, the novel cell type can be easily identified in other datasets profiled from the same tissue (for example, kidney). A simple classifier, such as a logistic classifier, is trained to predict cell types from universal cell embeddings, and is then applied to embeddings from other datasets of the same tissue (kidney), to confirm the cell type's existence and improve its characterization. (3) Finally, the same simple classifier can be applied to the embeddings of cells from any other tissue, to find cell types with similar biological functions or patterns of gene expression. (b) Identification of novel Norn cells in mouse kidney. UMAP visualization of zero-shot embedding of mouse renal cells from Kragesteen et al. [47]. Norn cells form a distinct cluster within the embedding space (circled). (c) Identification of Norn cells and Norn-like cells across tissues. A logistic classifier is trained to predict Norn cells from universal cell embeddings, and is then applied to other kidney datasets (left) and datasets from lung and heart (right). The log fold change of known Norn marker genes between cells predicted to be Norn cells and the remaining cells within each dataset is visualized. Cells which are predicted to be Norn-like preferentially express Norn markers in kidney, as well as in lung and heart. Notably, *Cxcl14* has a mixed pattern of expression among some datasets. (d) Cells predicted to be Norn-like cells within a lung disease dataset [49] express known Norn markers, as demonstrated by log fold change (LFC). (e) Differential gene expression in predicted Norn-like cells, grouped by disease status. There are significant differences in gene expression between cells from IPF, COPD and control patients. Patients with IPF and COPD are known to have elevated levels of blood stream *Epo*, with COPD patients having greater bloodstream *Epo* levels than patients with IPF.

590 **Data availability**

591 The full list of datasets used to train UCE are in Extended Data Table 2. Most of these datasets are
592 available to download from CellXGene [37]. Tabula Sapiens v2, used for model evaluation, will
593 be made available upon publication.

594 Datasets analyzed in the paper are publicly available to download. The green monkey lung
595 and lymph node dataset is available with accession code GSE156755. The naked mole rat dataset
596 is available with accession code GSE132642. The chicken retina dataset is available with acces-
597 sion code GSE159107. The chicken heart dataset is available with accession code GSE149457.
598 The mouse kidney dataset is available with accession code GSE193321. The human lung disease
599 dataset is available with accession code GSE136831.

600 **Code availability**

601 UCE was written in Python using the PyTorch library. The source code is available on Github at
602 <https://github.com/snap-stanford/uce>.

603 **Acknowledgements**

604 We thank Rok Sosič, Kexin Huang, Charlotte Bunne, Hanchen Wang, Michihiro Yasunaga, Michael
605 Moor, Minkai Xu, Mika Jain, George Crowley, Maria Brbić, Jonah Cool, Nicholas Sofroniew,
606 Andrew Tolopko, Ivana Jelic, Ana-Maria Istrate and Pablo Garcia-Nieto for discussions and for
607 providing feedback on our manuscript. We acknowledge support from Robert C. Jones for help
608 with accessing and analyzing the Tabula Sapiens v2 dataset. We acknowledge support from the
609 Chan Zuckerberg Initiative, including help with accessing and processing CxG datasets. We grate-
610 fully acknowledge the support of DARPA under Nos. N660011924033 (MCS); NSF under Nos.
611 OAC-1835598 (CINES), CCF-1918940 (Expeditions), Stanford Data Science Initiative, Wu Tsai
612 Neurosciences Institute, Amazon, Genentech, GSK, Hitachi, Juniper Networks, and KDDI. Y.
613 RH. acknowledges funding support from GlaxoSmithKline. L.S. was supported by the American
614 Slovenia Education Foundation (ASEF). Icons created with BioRender.com.

615 **Author information**

616 Y.R.S., Y.R.H., S.Q. and J.L. conceived the study. Y.R.S., Y.R.H., S.Q. and J.L. performed research,
617 contributed new analytical tools, designed algorithmic frameworks, analyzed data and wrote the
618 manuscript. Y.R.S. and Y.R.H. performed experiments and developed the software. A.A. and L.S.
619 contributed to code and performed analyses. T.S. provided annotated data.

References

- 620
621
622 1. Vaishnav, E. D. *et al.* The evolution, evolvability and engineering of gene regulatory dna.
623 *Nature* **603**, 455–463 (2022).
- 624 2. Onuchic, J. N., Luthey-Schulten, Z. & Wolynes, P. G. Theory of protein folding: the energy
625 landscape perspective. *Annual review of physical chemistry* **48**, 545–600 (1997).
- 626 3. Moris, N., Pina, C. & Arias, A. M. Transition states and cell fate decisions in epigenetic
627 landscapes. *Nature Reviews Genetics* **17**, 693–703 (2016).
- 628 4. Treutlein, B. *et al.* Reconstructing lineage hierarchies of the distal lung epithelium using
629 single-cell rna-seq. *Nature* **509**, 371–375 (2014).
- 630 5. Waddington, C. H. *The strategy of the genes* (Routledge, 1957).
- 631 6. Schaum, N. *et al.* Single-cell transcriptomics of 20 mouse organs creates a tabula muris: The
632 tabula muris consortium. *Nature* **562**, 367 (2018).
- 633 7. Regev, A. *et al.* The human cell atlas. *elife* **6**, e27041 (2017).
- 634 8. Rood, J. E., Maartens, A., Hupalowska, A., Teichmann, S. A. & Regev, A. Impact of the
635 human cell atlas on medicine. *Nature medicine* **28**, 2486–2496 (2022).
- 636 9. Tanay, A. & Regev, A. Scaling single-cell genomics from phenomenology to mechanism.
637 *Nature* **541**, 331–338 (2017).
- 638 10. Plass, M. *et al.* Cell type atlas and lineage tree of a whole complex animal by single-cell
639 transcriptomics. *Science* **360**, eaaq1723 (2018).
- 640 11. Consortium*, T. S. *et al.* The tabula sapiens: A multiple-organ, single-cell transcriptomic atlas
641 of humans. *Science* **376**, eabl4896 (2022).
- 642 12. Siletti, K. *et al.* Transcriptomic diversity of cell types across the adult human brain. *Science*
643 **382**, eadd7046 (2023).
- 644 13. Li, H. *et al.* Fly cell atlas: A single-nucleus transcriptomic atlas of the adult fruit fly. *Science*
645 **375**, eabk2432 (2022).
- 646 14. Eraslan, G., Avsec, Ž., Gagneur, J. & Theis, F. J. Deep learning: new computational modelling
647 techniques for genomics. *Nature Reviews Genetics* **20**, 389–403 (2019).
- 648 15. Lopez, R., Regier, J., Cole, M. B., Jordan, M. I. & Yosef, N. Deep generative modeling for
649 single-cell transcriptomics. *Nature methods* **15**, 1053–1058 (2018).
- 650 16. Luecken, M. D. *et al.* Benchmarking atlas-level data integration in single-cell genomics. *Na-*
651 *ture methods* **19**, 41–50 (2022).
- 652 17. Argelaguet, R., Cuomo, A. S., Stegle, O. & Marioni, J. C. Computational principles and
653 challenges in single-cell data integration. *Nature biotechnology* **39**, 1202–1215 (2021).
- 654 18. Lotfollahi, M. *et al.* Mapping single-cell data to reference atlases by transfer learning. *Nature*
655 *biotechnology* **40**, 121–130 (2022).

- 656 19. Tarashansky, A. J. *et al.* Mapping single-cell atlases throughout metazoa unravels cell type
657 evolution. *Elife* **10**, e66747 (2021).
- 658 20. Brown, T. *et al.* Language models are few-shot learners. *Advances in neural information*
659 *processing systems* **33**, 1877–1901 (2020).
- 660 21. OpenAI. Gpt-4 technical report (2023). [2303.08774](https://arxiv.org/abs/2303.08774).
- 661 22. Anil, R. *et al.* Palm 2 technical report. *arXiv preprint arXiv:2305.10403* (2023).
- 662 23. Touvron, H. *et al.* Llama: Open and efficient foundation language models. *arXiv preprint*
663 *arXiv:2302.13971* (2023).
- 664 24. Kirillov, A. *et al.* Segment anything. *arXiv preprint arXiv:2304.02643* (2023).
- 665 25. Bommasani, R. *et al.* On the opportunities and risks of foundation models. *arXiv preprint*
666 *arXiv:2108.07258* (2021).
- 667 26. Avsec, Ž. *et al.* Effective gene expression prediction from sequence by integrating long-range
668 interactions. *Nature methods* **18**, 1196–1203 (2021).
- 669 27. Rives, A. *et al.* Biological structure and function emerge from scaling unsupervised learning
670 to 250 million protein sequences. *Proceedings of the National Academy of Sciences* **118**,
671 e2016239118 (2021).
- 672 28. Theodoris, C. V. *et al.* Transfer learning enables predictions in network biology. *Nature* 1–9
673 (2023).
- 674 29. Cui, H. *et al.* scgpt: Towards building a foundation model for single-cell multi-omics using
675 generative ai. *bioRxiv* 2023–04 (2023).
- 676 30. Stegle, O., Teichmann, S. A. & Marioni, J. C. Computational and analytical challenges in
677 single-cell transcriptomics. *Nature Reviews Genetics* **16**, 133–145 (2015).
- 678 31. Quake, S. R. The cell as a bag of rna. *Trends in Genetics* **37**, 1064–1068 (2021).
- 679 32. Vaswani, A. *et al.* Attention is all you need. *Advances in neural information processing*
680 *systems* **30** (2017).
- 681 33. Lin, Z. *et al.* Evolutionary-scale prediction of atomic-level protein structure with a language
682 model. *Science* **379**, 1123–1130 (2023).
- 683 34. Rosen, Y. *et al.* Toward universal cell embeddings: integrating single-cell RNA-seq datasets
684 across species with SATURN. *Nature Methods* **21**, 1492–1500 (2024).
- 685 35. Devlin, J., Chang, M.-W., Lee, K. & Toutanova, K. Bert: Pre-training of deep bidirectional
686 transformers for language understanding. *arXiv preprint arXiv:1810.04805* (2018).
- 687 36. Wang, H., Leskovec, J. & Regev, A. Metric mirages in cell embeddings. *BioRxiv* (2024).
- 688 37. Biology, C. S.-C. *et al.* Cz cellxgene discover: A single-cell data platform for scalable explo-
689 ration, analysis and modeling of aggregated data. *bioRxiv* 2023–10 (2023).
- 690 38. Gordon, S., Plüddemann, A. & Martinez Estrada, F. Macrophage heterogeneity in tissues:
691 phenotypic diversity and functions. *Immunological reviews* **262**, 36–55 (2014).

- 692 39. Conde, C. D. *et al.* Cross-tissue immune cell analysis reveals tissue-specific features in hu-
693 mans. *Science* **376**, eabl5197 (2022).
- 694 40. Speranza, E. *et al.* Single-cell rna sequencing reveals sars-cov-2 infection dynamics in lungs
695 of african green monkeys. *Science translational medicine* **13**, eabe8146 (2021).
- 696 41. Hilton, H. G. *et al.* Single-cell transcriptomics of the naked mole-rat reveals unexpected
697 features of mammalian immunity. *PLoS Biology* **17**, e3000528 (2019).
- 698 42. Yamagata, M., Yan, W. & Sanes, J. R. A cell atlas of the chick retina based on single-cell
699 transcriptomics. *Elife* **10**, e63907 (2021).
- 700 43. Mantri, M. *et al.* Spatiotemporal single-cell rna sequencing of developing chicken hearts iden-
701 tifies interplay between cellular differentiation and morphogenesis. *Nature communications*
702 **12**, 1771 (2021).
- 703 44. Orozco, L. D. *et al.* Integration of eQTL and a single-cell atlas in the human eye identifies
704 causal genes for age-related macular degeneration. *Cell reports* **30**, 1246–1259.e6 (2020).
- 705 45. Li, H. *et al.* Fly cell atlas: A single-nucleus transcriptomic atlas of the adult fruit fly. *Science*
706 **375**, eabk2432 (2022).
- 707 46. Bard, J., Rhee, S. Y. & Ashburner, M. An ontology for cell types. *Genome biology* **6**, 1–5
708 (2005).
- 709 47. Kragesteen, B. K. *et al.* The transcriptional and regulatory identity of erythropoietin producing
710 cells. *Nature medicine* 1–10 (2023).
- 711 48. Haine, L. *et al.* Cytoprotective effects of erythropoietin: What about the lung? *Biomedicine*
712 *& Pharmacotherapy* **139**, 111547 (2021).
- 713 49. Adams, T. S. *et al.* Single-cell rna-seq reveals ectopic and aberrant lung-resident cell popula-
714 tions in idiopathic pulmonary fibrosis. *Science advances* **6**, eaba1983 (2020).
- 715 50. Tassiopoulos, S. *et al.* Erythropoietic response to hypoxaemia in diffuse idiopathic pulmonary
716 fibrosis, as opposed to chronic obstructive pulmonary disease. *Respiratory Medicine* **95**, 471–
717 475 (2001).
- 718 51. Abdel-Aziz, C., Okaily, N. & Kasem, A. Erythropoietin: role in idiopathic pulmonary fibrosis
719 revisited. *The Egyptian Journal of Chest Diseases and Tuberculosis* **69**, 716 (2020).
- 720 52. Tsantes, A. E. *et al.* Red cell macrocytosis in hypoxemic patients with chronic obstructive
721 pulmonary disease. *Respiratory medicine* **98**, 1117–1123 (2004).
- 722 53. Safran, M. *et al.* The GeneCards suite. In Abugessaisa, I. & Kasukawa, T. (eds.) *Practical*
723 *guide to life science databases*, 27–56 (Springer Singapore, Singapore, 2021).
- 724 54. Stelzer, G. *et al.* The genecards suite: from gene data mining to disease genome sequence
725 analyses. *Current Protocols in Bioinformatics* **54**, 1.30.1–1.30.33 (2016).
- 726 55. Piran, Z., Cohen, N., Hoshen, Y. & Nitzan, M. Disentanglement of single-cell data with
727 biolord. *Nature Biotechnology* (2024).
- 728 56. Piran, Z. & Nitzan, M. SiFT: uncovering hidden biological processes by probabilistic filtering
729 of single-cell data. *Nature Communications* **15**, 760 (2024).

- 730 57. Lopez, R. *et al.* Learning causal representations of single cells via sparse mechanism shift
731 modeling. In van der Schaar, M., Zhang, C. & Janzing, D. (eds.) *Proceedings of the Second*
732 *Conference on Causal Learning and Reasoning*, vol. 213 of *Proceedings of Machine Learning*
733 *Research*, 662–691 (PMLR, 2023).
- 734 58. Kunes, R. Z., Walle, T., Land, M., Nawy, T. & Pe'er, D. Supervised discovery of interpretable
735 gene programs from single-cell data. *Nature Biotechnology* **42**, 1084–1095 (2024).
- 736 59. Amaral, P. *et al.* The status of the human gene catalogue. *Nature* **622**, 41–47 (2023).
- 737 60. Brenner, S. Nature's gift to science (nobel lecture). *Chembiochem* **4**, 683–687 (2003).
- 738 61. Gu, A., Goel, K. & Ré, C. Efficiently modeling long sequences with structured state spaces.
739 *arXiv* (2021).
- 740 62. Wolf, F. A., Angerer, P. & Theis, F. J. SCANPY: large-scale single-cell gene expression data
741 analysis. *Genome Biology* **19**, 15 (2018).
- 742 63. Shen, H. *et al.* Generative pretraining from large-scale transcriptomes for single-cell decipher-
743 ing. *iScience* **26**, 106536 (2023).